Transfer Molding of Nanoscale Oxides Using Water-Soluble Templates

John D. Bass,[†] Charles D. Schaper,[‡] Charles T. Rettner,[†] Noel Arellano,[†] Fahhad H. Alharbi,[§] Robert D. Miller,[†] and Ho-Cheol Kim[†,*]

[†]IBM Almaden Research Center, 650 Harry Road, San Jose, California 95120, United States, [‡]Transfer Devices, Inc., 500 Laurelwood Road, Suite 11, Santa Clara, California 95054, United States, and [§]The National Nanotechnology Center, King Abdulaziz City for Science and Technology, P. O. 6086, Riyadh 11442, Saudi Arabia

ABSTRACT We report a facile method for creating nanoscopic oxide structures over large areas that is capable of producing high aspect ratio nanoscale structures with feature sizes below 50 nm. A variety of nanostructured oxides including TiO_2, SnO_2 and organosilicates are formed using sol–gel and nanoparticle precursors by way of molding with water-soluble polymeric templates generated from silicon masters. Sequential stacking techniques are developed that generate unique 3-dimensional nanostructures with combinatorially mixed geometries, scales, and materials. Applicable to a variety of substrates, this scalable method allows access to a broad range of new thin film morphologies for applications in devices, catalysts, and functional surface coatings.

KEYWORDS: nanostructures · metal oxides · titania · microtransfer molding · multilayered structures

Metal oxides feature prominently in a number of next-generation high-tech domains including photonics,[1] membranes,[2] biological supports,[3–5] sensing,[6,7] electrochromics,[8] and environmental applications[9] including photoelectrolysis of water[10] and catalytic and photocatalytic applications.[11–14] In many of these emerging areas, there is keen interest in the ability to create nanometer scale structures, especially one-dimensional structures that provide high surface areas and low tortuosity for improved transport characteristics. In addition, high surface areas, easy reagent accessibility, and direct-paths for electrical transport make such 1D structures ideal for many electrochemical applications. Further advantages provided by short radial diffusion and increased mechanical stability are of interest for lithium insertion for high performance batteries.[15,16] In photocatalytic, photoelectrolysis, and photovoltaics applications, including radial *p–n* junction nanorod solar cells, these structures can provide a means to increase efficiency in transport limited systems by allowing radial transport to occur perpendicular to light absorption.[17,18]

A variety of methods have been developed to synthesize 1D nanostructured metal oxides. Solution phase and hydrothermal growth of crystalline rods,[19–24] oxidation,[25,26] or anodization[27] of metal foils, vapor phase growth,[28,29] and block copolymer templating[30–33] are common strategies. In contrast to these bottom-up strategies, the ability to directly pattern high aspect ratio 1-D metal oxides through transfer molding (TM) holds a number of inherent advantages. These include broader and more flexible control over the patterning, easier device integration, lower operating and materials cost, and the potential for high throughput manufacturing including roll-to-roll production. Demonstration of a TM approach for the production of high aspect ratio nanoscale metal oxides with features below 50 nm is an important milestone in this domain.

Submicrometer patterning of titanium silicates has been demonstrated using PDMS soft lithography,[34] and extended using perfluoropolyether (PFPEs) elastomers. The improved filling and release characteristics based on the low surface energy of PFPEs has been used to pattern a variety of oxides and mixed metal oxides,[35] with sub 200 nm features and aspect ratios of up to 2.5.[35]

Interest in patterning oxide features at even smaller scales and larger aspect ratios led us to investigate water-soluble poly(vinyl alcohol) (PVA) as a template material.[36–38] In this approach, water-soluble PVA templates, prepared *en masse* from hard template masters such as large area lithographically patterned silicon, are used to create structured oxides. The PVA template is filled with a solution-phase oxide precursor, laminated to a substrate, and, after partial curing of the precursor (heat, UV, *etc.*), subsequently dissolved away. This process is shown schematically in Figure 1 for TiO_2. In addition to the positive environmental aspects of water-based processing and the avoidance of fluorocarbons, removal of the template by

* Address correspondence to hckim@us.ibm.com.

Received for review February 16, 2011 and accepted April 6, 2011.

Published online April 06, 2011
10.1021/nn2006514

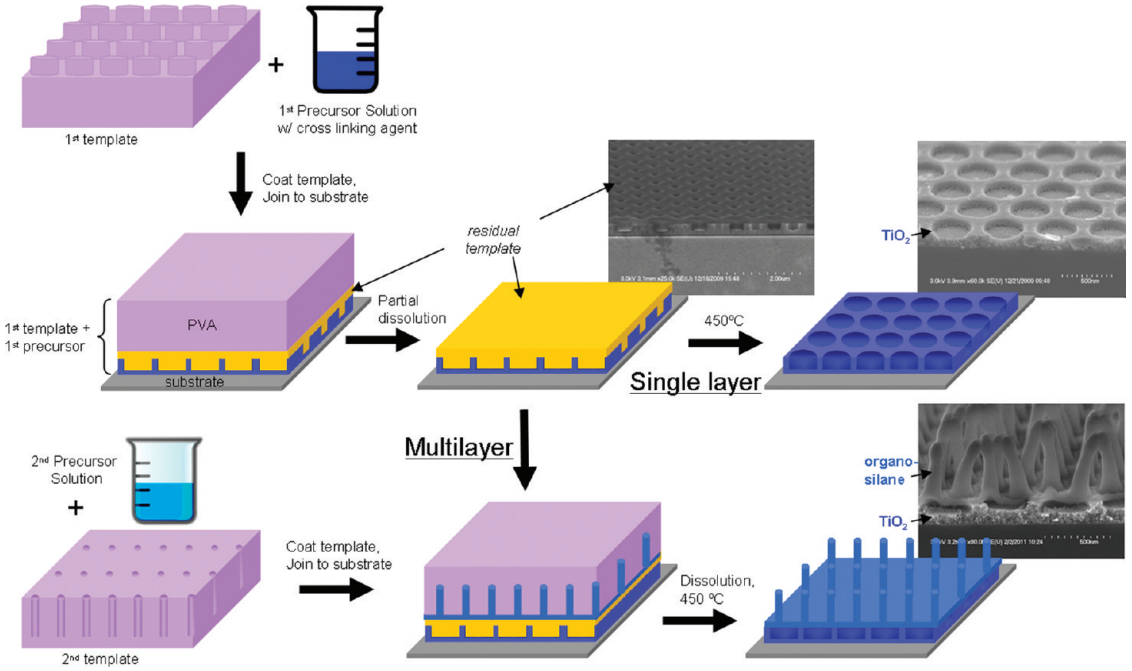

Figure 1. Schematic representation of transfer molding (TM) of nanostructured oxides using water-soluble polymer (polyvinyl alcohol) templates.

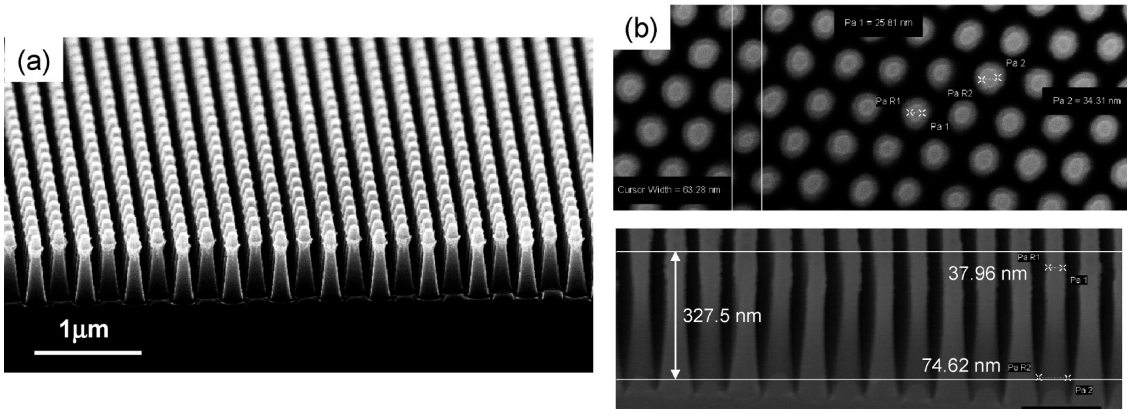

Figure 2. SEM micrograph of a typical silicon master used to create PVA daughter templates. For (a) the large-feature size master, pillars are ~135 nm in width at half-height, 750 nm tall, and 275 nm center-to-center. The smaller feature size master (b) has pillars of ~50 nm in width at half-height, and 330 nm in height.

dissolution is an inherently softer release approach than mechanically peeling off the template. In this paper, we report the creation of scalable nanostructures of metal oxides with single and multilayered structures on substrates.

RESULTS AND DISCUSSION

The approach employed was to create disposable, water-soluble PVA templates from large-area silicon masters. Two patterns on silicon wafers, one with 135 nm and another with 50 nm features were prepared by lithography followed by plasma etching. The master containing pillars of ~135 nm in diameter at half-height, 750 nm tall, and a 275 nm center-to-center spacing was prepared using conventional optical lithography. The master containing 50 nm diameter pillars was made using electron beam lithography together with a lift-off process to produce a Cr hardmask, followed by reactive ion etching into the oxide substrate. Figure 2 shows SEM micrographs of silicon masters of 135 nm pillars (a) and 50 nm pillars (b). It is noted that the sidewall profile of the pillars is not perfectly vertical, which results in the opposite tone PVA templates having nonvertical pores upon molding.

Following the approach of Figure 1, we first used the PVA template for fabricating TiO_2 nanostructures. A sol–gel solution containing *n*-butyl polytitanate (Tyzor BTP, DuPont), acetylacetone, and acetic acid is spin-coated onto the PVA templates. The coated template was bonded to a substrate and exposed to UV radiation to induce partial condensation of the TiO_2 precursor.

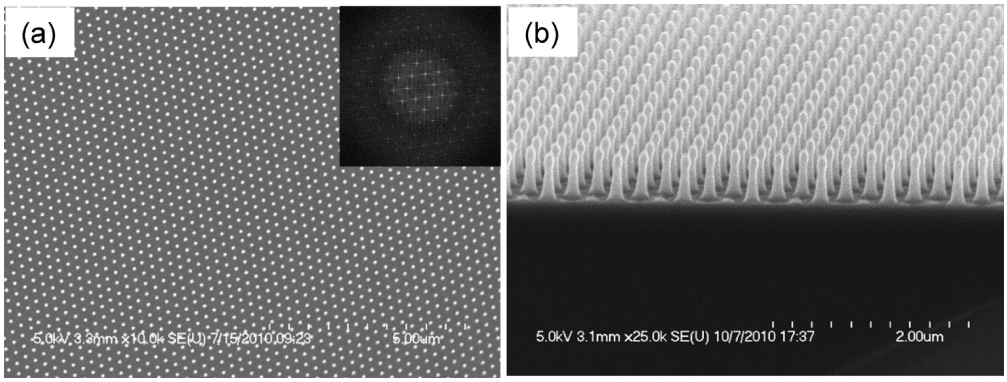

Figure 3. High aspect ratio TiO_2 pillars ~70 nm in width at half-height, ~340 nm in length, and covering large areas created by microtransfer molding using a PVA template.

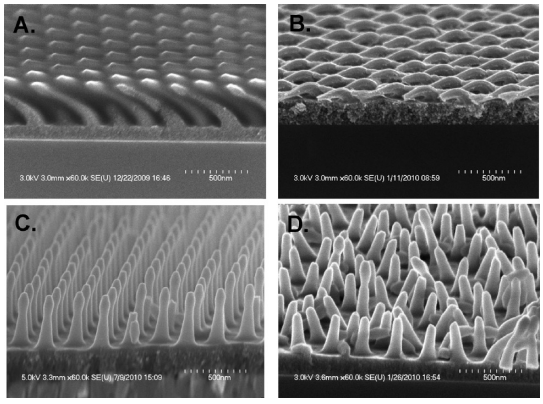

Figure 4. (a) Intermediate structures formed after dissolution of the PVA using sol–gel formulations without acetic acid; (b) without acetic acid large-scale uniform folding and pillar breakage is seen in the final material after calcination; (c) intermediate structures formed after dissolution of the PVA using sol–gel formulations with acetic acid; and (d) starting from titania clusters.

Exposure to warm water dissolved the PVA template leaving a partially condensed network of nanostructured TiO_2. Calcination by thermal treatment to 450 °C resulted in polycrystalline TiO_2 pillars. Figure 3 shows SEM micrographs of TiO_2 pillars prepared using the 135 nm PVA template. Owing to volumetric shrinkage of the sol–gel TiO_2 precursor during calcination (approximately 45–50% shrinkage), the final TiO_2 pillars are ~70 nm in width at half-height and are ~340 nm in height. The pillars are seen by FFT analysis to have a very high degree of ordering.

It should be noted that the presence of acetic acid in the precursor solution is critical in achieving high aspect ratio structures. Without the added acid, complete removal of the PVA is not achieved upon water treatment as shown in Figure 4a. Upon calcination, this interstitial residue causes a large-scale, uniform collapse of the pillars resulting in folded structures as shown in Figure 4b. These folded structures often span hundreds of square micrometers and are highly uniform as observed by FFT analysis of top-view SEM micrographs (Supporting Information).

With the addition of acetic acid to the precursor solution, PVA is effectively removed from the interstitial regions to give fully isolated pillars after water dissolution (Figure 4c). These isolated pillars do not collapse during calcination, and behavior from pillar to pillar remains uncorrelated. To further investigate these phenomenon, ethanolic $TiCl_4$ and $Ti_8O_8((CH_3)_3CCOO)_{16}$ titania clusters were used as titania precursors. At low water content ($H_2O/Ti < 3$) condensation is suppressed in the ethanolic $TiCl_4$ system and the titania species remain molecular as opposed to oligomeric.[39] The $TiCl_4$-based system leads to a nearly identical interstitial material observed with sol–gel type TiO_2 precursor after dissolution. The titania cluster[40] consists of a Ti_8O_8 ring structure with eight axial and eight equatorial pivalate ligands. For these clusters, though they are less adept at registering the template features, no interstitial material is observed as shown in Figure 4d. These results suggest that in the acetic acid system, as well as with the larger and relatively stable titania clusters, increased condensation of Ti centers decreases diffusion into the PVA template. Diffusion of titania precursors very likely causes a reaction with the abundant OH groups of the PVA, effectively cross-linking the PVA and inhibiting dissolution. The PVA/titania residue in the interstitial material binds neighboring pillars together resulting in highly correlated movement causing pillar breakage. Tensile forces in this interstitial space during calcination, either as capillary action upon water removal or upon volume reduction from further cross-linking or removal of the PVA, leads to coordinated folding and collapse over large areas.

Transfer molding at sub 50 nm feature sizes introduces a number of potential challenges both in the production of the PVA templates and in the production of the templated metal oxides. The former includes difficulties filling the silicon master with PVA and release after molding. The latter includes filling the oxide precursors, diffusion, the cross-linking of precursors with PVA, shrinkage, mechanical stability, and so on. Using identical sol–gel TiO_2 precursors as above in the presence of acetic acid, templating can be

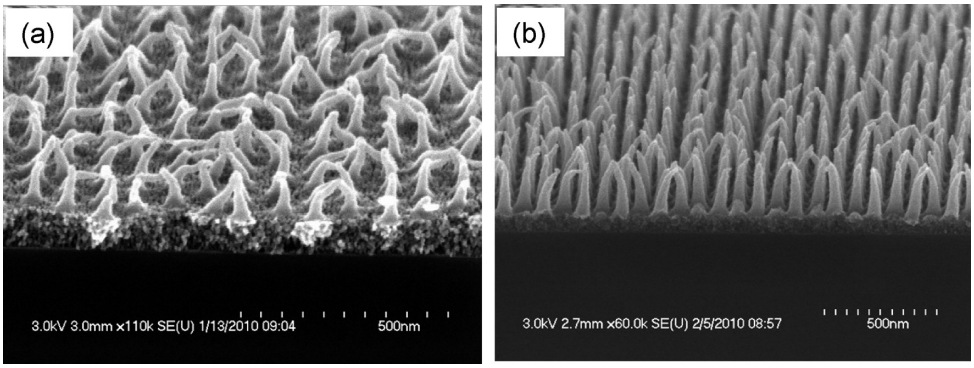

Figure 5. SEM micrographs of templated pillars at sub-50 nm feature sizes using (a) sol−gel titania with acetic acid and (b) TiO_2 nanorods.

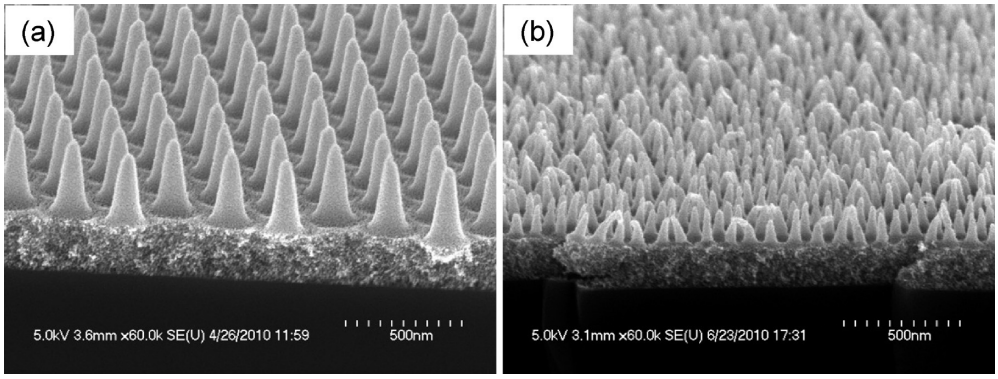

Figure 6. SEM micrographs of templated SnO_2 pillars using (a) the 135 nm template and (b) the 50 nm template.

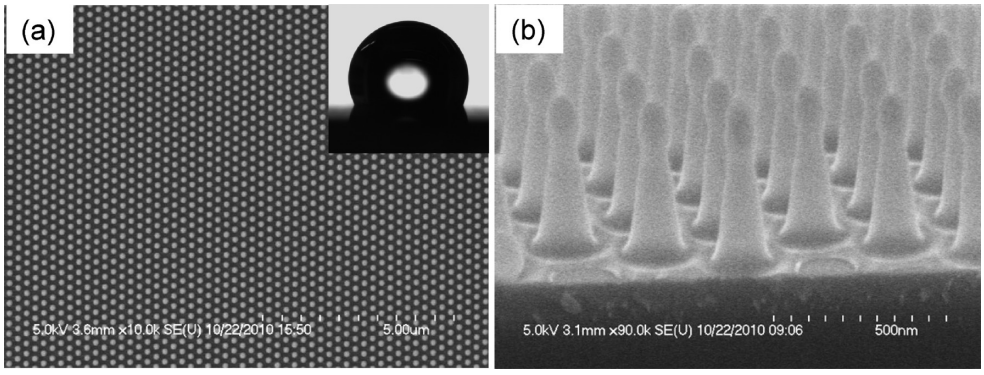

Figure 7. (a) Top view and (b) cross-section SEM micrographs of templated organosilicate pillars. (Inset) Water contact angle measurement show a hydrophobic surface.

achieved at very small scales with pillars of approximately 25 nm in width at half-height and ~100 nm in length with center-to-center distances of 100 nm as shown in Figure 5a. The pillars are not rigid, however, and many are significantly folded reducing the effective aspect ratio. Switching to presynthesized nanomaterials such as nanoparticles and nanorods improved the mechanical stability of the templated features and reduced the shrinkage during calcination. Figure 5b shows a SEM micrograph of TiO_2 nanopillars molded using presynthesized nanorods capped with oleic acid.[41] The resulting pillars are ~45 nm at half-height and have lengths of ~220 nm, yielding aspect ratios of almost 5 and good coverage over large areas.

To explore the generality of this approach, we fabricated tin oxide (SnO_2) nanopillars by the TM method using both the 135 and 50 nm templates as shown in Figure 6. Similar to our approach for the 50 nm TiO_2 pillars, we used presynthesized SnO_2 nanoparticles capped with oleic acid ligands.[42] Compared to TiO_2, the resulting SnO_2 pillars show very low shrinkage based on the horizontal dimensions, but poorer aspect ratios possibly due to problems filling of the template past the necked portion of the PVA template. It is noted

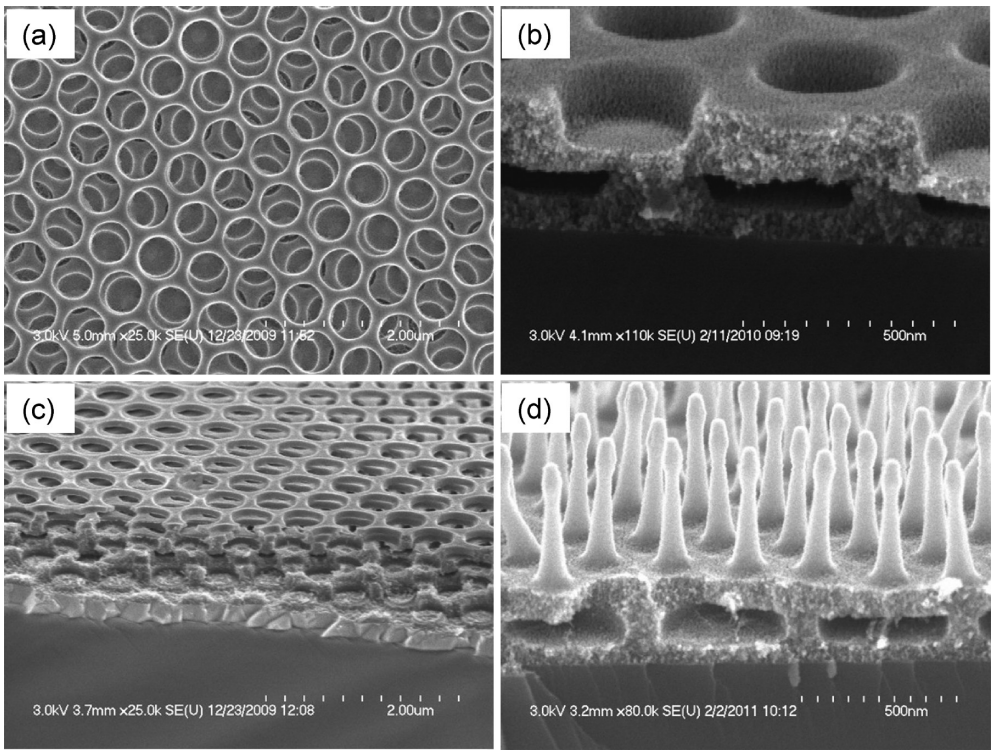

Figure 8. SEM micrographs of (a) a top view of an open-cell two-layer titania structure formed using a 200 nm diameter mesh template, (b) a cross-section of a closed-cell two-layer structure with a titania first layer and a SnO_2 second layer, (c) a cross-section of a five layer titania structure, and (d) a cross-section of a two-layer titania structure formed using two different templates, the mesh template and a post template.

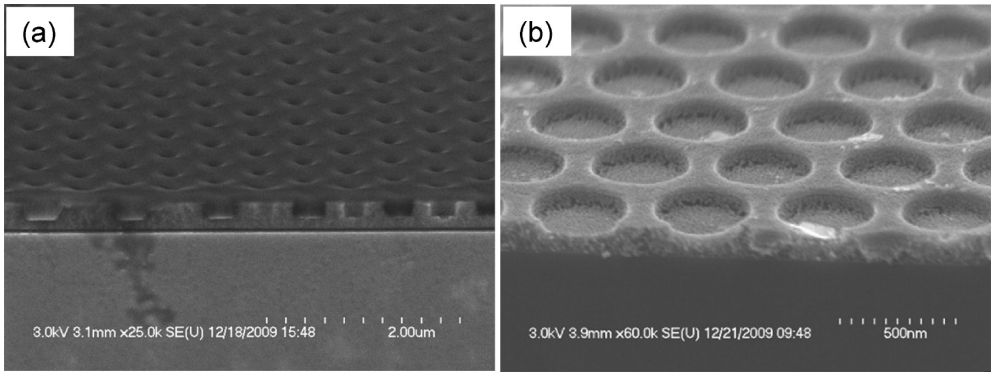

Figure 9. (a) SEM micrograph of a templated titania structure prepared without acetic acid after the dissolution step. The interstitial PVA material is clearly visible locally confined in and around the templated features. Calcination to 450 °C reveals more clearly (b) the underlying templated structure.

that this PVA approach can be generally used for nanostructuring other types of inorganic materials. For example, Figure 7 panels a and b show templated organosilicates. These materials, fabricated using a silsesquioxane organosilicate precursor,[31] show even lower shrinkage, yielding structures that are ~460 nm in height and 110 nm in diameter. Because of the hydrophobicity of cross-linked organosilicates and nanostructures, the surface of nanopillars shows ultrahydrophobic behavior. As shown in the inset in Figure 7a, water contact angel of 115 ± 2 degrees was observed with the pillars generated with 135 nm template.

Successive stacking of transfer molded layers can be used to generate films containing closed- and open-cell nanostructures. This approach can be extended to mixed materials and mixed templates as schematically represented in Figure 1 (see multilayer route in Figure 1). Starting from a template that produces a 200 nm diameter mesh, both open-cell (Figure 8a,c) and closed-cell (Figure 8b,d) stacked structures are possible. Closed-cell structures are formed when the quantity of precursor is greater than the volume of the template. Figure 8b also illustrates the stacking of two different materials, TiO_2 for the first layer, and SnO_2 for

the second layer (see also Figure 1 where organosilicate posts are stacked on a TiO_2 mesh). Stacking can be repeated multiple times; Figure 8c shows a cross-section of a fractured five-layer TiO_2 structure. Different types of templates may also be combined such as the mesh template and the post templates mentioned earlier, Figure 8d.

Subsequent layers are put down directly on the intermediate structure that exists after the dissolution step. TiO_2 formulations without acetic acid are used for the underlayers so that cross-linked interstitial PVA remains in and around the nascent templated titania structures (Figure 9a). Retaining this organic material in the pores is believed to inhibit draining and infill[43] that can occur with fluid materials and to prevent vertical mixing of the patterned features[35] that may otherwise occur with soft templates. The organic material is eventually removed during a final calcination step, revealing the underlying pattern, as demonstrated for a single layer in Figure 9b.

CONCLUSIONS

We have shown that high aspect ratio metal oxide pillars can be successfully prepared on a variety of substrates using an environmentally friendly, water based PVA TM approach. The creation of organosilicate, TiO_2, and SnO_2 pillars is demonstrated, with achievable feature sizes below 50 nm and aspect ratios reaching nearly 5 to 1. Unique stacked oxide structures using different material and template combinations are also accessible. This approach, using sacrificial water-soluble templates represents a low cost flexible route for the patterning of oxide materials relevant for device fabrication.

EXPERIMENTAL SECTION

The master containing pillars of ~135 nm in diameter at half-height, 750 nm tall, and a 275 nm center-to-center spacing was prepared using conventional optical lithography. A 4× photomask of a field size 80 mm × 80 mm was used within an ASML 1400 photolithography tool to produce 135 nm diameter pillars at the imaging plane in photoresist stepped across the surface of a 200 nm thick SiO_2 layer deposited on a 300 mm silicon wafer. The step size of the photolithography tool was calibrated so as to minimize the stitching error of the pillars, arranged in a triangular array, along the boundary of the imaging field over the 300 mm wafer. After wet development of the resist, plasma etching was used to etch through the oxide layer, using silicon as the etch stop, to form the 135 nm diameter pillars, 200 nm tall, in oxide on silicon after ashing the resist. The oxide patterns were used as an etch mask for subsequent plasma etching for silicon to obtain a high aspect ratio master. Residual oxide was removed by rinsing with an HF solution.

The master containing 50 nm diameter pillars was made using electron beam lithography together with a liftoff process. We employed a high resolution positive tone electron beam resist (ZEP-520A, Nippon Zeon) coated to 95 nm on a five inch silicon wafer with a 1 μm thick thermal silicon dioxide film, followed by a post-apply bake of 175 °C for 3 min. The pattern consisted of a hexagonal array of 60 nm diameter circles with a period of 100 nm, written with a Leica VB6 HR electron-beam lithography tool at a dose of ~3 mC/cm^2 at a beam current of ~5 nA. The exposed resist was then developed at 0.6 °C in amyl acetate for 3 min followed by quench in a room temp solution of 1:3 methyl isobutyl ketone−isopropyl alcohol (IPA) for 30 s, and finally rinsed with IPA for 10 s. Next a 30 nm thick Cr thin film was evaporated onto the resist pattern to create a hardmask for a subsequent reactive ion etch step. The Cr film was lifted off in a 55 °C bath of *N*-methylpyrrolidone (NMP) with sonic agitation for 40 min and rinsed in IPA followed by a rinse in deionized water. After the lift-off process the oxide wafer was etched using inductively coupled CF_4 plasma for 4 min (3mT chamber pressure, 20 sccm CF_4 flow rate, 200 W coil power, and 35 W platen power). Then the Cr hardmask was removed at room temperature using Cyantek CR-14 etchant followed by a water rinse. The wafer was then placed in a 60 °C bath of EKC265 (DuPont) to remove metallic and organic residue. Finally the wafer was cleaned in a 55 °C bath of NMP for 20 min, rinsed in IPA and water, and finally cleaned for 10 s in a downstream oxygen plasma reactor.

All chemicals and materials were obtained commercially or were synthesized using known procedures. ^{1}H NMR spectra were obtained at room temperature on an Avance 400 spectrometer in either *d*-toluene or *d*-$CHCl_3$. TiO_2 clusters and TiO_2 nanorods were synthesized by known procedures.[40,41,44] SEM was performed on a Hitachi S-4700 at 3 kV or on LEO 1550 VP at 15 kV. TEM images were recorded by JEOL-JEM 2010 electron microscopy operated at 200 kV.

Oleic acid capped SnO_2 nanoparticles were synthesized by adding 2.92 g tin(IV) *tert*-butoxide (7.1 mmol, Aldrich 99.99% grade) to 7.6 g degassed oleic acid (27 mmol, Aldrich technical grade, 90%) at room temperature. The mixture was heated to 270 °C over 20 min and held for a further 2 min before allowing it to cool to room temperature. The solution was then diluted with 30 mL of hexane and precipitated with ethanol. Further washing (3×) *via* precipitation dissolution with hexane/ethanol yielded ~0.6 g material that was easily solubilized with toluene.

The photosensitive titania precursor is an oligomeric titanate (OT) prepared from a acetylacetone chelated titanium alkoxide.[32,45] The solution (1:1 mol Ti/HAcAc) was diluted to 30 wt % in propylene glycol propyl ether (PGPE). Acetic acid (5 wt %) was added, and templates were prepared by spin coating this solution onto a PVA daughter at 2000 rpm for 45 s. The template was heated to 80 °C for 10 s before transferring onto a bare silicon wafer substrate (many other substrates are also suitable including transparent conducting oxides (TCOs) and sol−gel TiO_2-coated Si and TCOs). After an additional 10 s, the sample was removed and exposed to short wavelength UV illumination (245 nm) at room temperature for 20 to 30 min. Dissolution of the PVA backing was carried out at 42−85 °C (pH 4−7) for 25 min. The film was rinsed with water then dried with ethanol and nitrogen. Final calcination to remove the insoluble PVA material between the patterned titania was carried out at 450 °C for 2 h (ramp up at 5 °C/min). Templates from precursor solutions of $TiCl_4$ (18 wt % in ethanol), titania clusters (10 wt % in 50/50 v/v PGPE/toluene), and TiO_2 nanorods (5 wt % in toluene), were prepared in the same manner. SnO_2 nanoparticles (15 wt % in toluene) and templated organosilicates (30 wt % solutions in PGPE plus 5 vol % triethylamine relative to the total) were prepared similarly except that substrates were held at 80 °C for 20 min after transfer in lieu of treating with UV illumination.

Closed-cell two-layer structures fabricated with titania and tin oxide using a 250 nm mesh PVA mold. A 30 wt % titania precursor solution consisting of Dupont Tyzor BTP and acetylacetone (1:1 mol Ti/mol HAcAc) in PGPE was used to mold the first layer following the procedures outlined above. A tin oxide second layer was molded using a 20 wt % solution as outlined above. Open-celled titania structure were fabricated using a 13 wt % titania precursor solution.

Acknowledgment. We are grateful to Dr. Y. Zhang who worked at IBM T. J. Watson Research Center for preparing silicon masters.

Supporting Information Available: Top-view SEM micrographs and FFT analysis of domains of highly uniform collapsed structures spanning hundreds of square micrometers. This material is available free of charge *via* the Internet at http://pubs.acs.org.

REFERENCES AND NOTES

1. Subramania, G.; Lee, Y.-J.; Fischer, A. J.; Koleske, D. D. Log-Pile TiO_2 Photonic Crystal for Light Control at Near-UV and Visible Wavelengths. *Adv. Mater.* **2010,** *22*, 487–491.
2. Guliants, V. V.; Carreon, M. A.; Lin, Y. S. Ordered Mesoporous and Macroporous Inorganic Films and Membranes. *J. Membr. Sci.* **2004,** *235*, 53–72.
3. Bass, J. D.; Belamie, E.; Grosso, D.; Boissiere, C.; Coradin, T.; Sanchez, C. Nanostructuration of Titania Films Prepared by Self-Assembly to Affect Cell Adhesion. *J. Biomed. Mater. Res. A.* **2009,** *93A*, 96–106.
4. Bass, J. D.; Grosso, D.; Boissiere, C.; Belamie, E.; Coradin, T.; Sanchez, C. Stability of Mesoporous Oxide and Mixed Metal Oxide Materials under Biologically Relevant Conditions. *Chem. Mater.* **2007,** *19*, 4349–4356.
5. Yan, X. X.; Yu, C. Z.; Zhou, X. F.; Tang, J. W.; Zhao, D. Y. Highly Ordered Mesoporous Bioactive Glasses with Superior *in Vitro* Bone-Forming Bioactivities. *Angew. Chem., Int. Ed.* **2004,** *43*, 5980–5984.
6. Nicole, L.; Boissiere, C.; Grosso, D.; Hesemann, P.; Moreau, J.; Sanchez, C. M. Advanced Selective Optical Sensors Based on Periodically Organized Mesoporous Hybrid Silica Thin Films. *Chem. Commun.* **2004,** *20*, 2312–2313.
7. Wirnsberger, G.; Scott, B. J.; Stucky, G. D. pH Sensing with Mesoporous Thin Films. *Chem. Commun.* **2001,** *1*, 119–120.
8. Ohsuku, T.; Hirai, T. An Electrochromic Display Based on Titanium Dioxide. *Electrochim. Acta* **1982,** *27*, 1263–1266.
9. Bosc, F.; Edwards, D.; Keller, N.; Keller, V.; Ayral, A. Mesoporous TiO_2-Based Photocatalysts for UV and Visible Light Gas-Phase Toluene Degradation. *Thin Solid Films* **2006,** *495*, 272–279.
10. Fujishima, A.; Honda, K. Electrochemical Photolysis of Water at a Semiconductor Electrode. *Nature* **1972,** *238*, 37–38.
11. Fujishima, A.; Rao, T. N.; Tryk, D. A. Titanium Dioxide Photocatalysis. *J. Photochem. Photobiol. C* **2000,** *1*, 1–21.
12. Martinez-Ferrero, E.; Sakatani, Y.; Boissiere, C.; Grosso, D.; Fuertes, A.; Fraxedas, J.; Sanchez, C. Nanostructured Titanium Oxynitride Porous Thin Films as Efficient Visible-Active Photocatalysts. *Adv. Funct. Mater.* **2007,** *17*, 3348–3354.
13. Sakatani, Y.; Grosso, D.; Nicole, L.; Boissiere, C.; Soler-Illia, G. J. D. A.; Sanchez, C. Optimised Photocatalytic Activity of Grid-like Mesoporous TiO_2 Films: Effect of Crystallinity, Pore Size Distribution, and Pore Accessibility. *J. Mater. Chem.* **2006,** *16*, 77–82.
14. Hoffmann, M. R.; Martin, S. T.; Choi, W.; Bahnemann, D. W. Environmental Applications of Semiconductor Photocatalysis. *Chem. Rev.* **1995,** *95*, 69–96.
15. Chan, C. K.; Peng, H.; Liu, G.; McIlwrath, K.; Zhang, X. F.; Huggins, R. A.; Cui, Y. High-Performance Lithium Battery Anodes Using Silicon Nanowires. *Nat. Nanotechnol.* **2008,** *3*, 31–35.
16. Gao, X.; Zhu, H.; Pan, G.; Ye, S.; Lan, Y.; Wu, F.; Song, D. Preparation and Electrochemical Characterization of Anatase Nanorods for Lithium-Inserting Electrode Material. *J. Phys. Chem. B* **2004,** *108*, 2868–2872.
17. Kannan, B.; Castelino, K.; Majumdar, A. Design of Nanostructured Heterojunction Polymer Photovoltaic Devices. *Nano Lett.* **2003,** *3*, 1729–1733.
18. Kayes, B. M.; Atwater, H. A.; Lewis, N. S. Comparison of the Device Physics Principles of Planar and Radial $p-n$ Junction Nanorod Solar Cells. *J. Appl. Phys.* **2005,** *97*, 114302–11.
19. Hosono, E.; Fujihara, S.; Kakiuchi, K.; Imai, H. Growth of Submicrometer-Scale Rectangular Parallelepiped Rutile TiO_2 Films in Aqueous $TiCl_3$ Solutions under Hydrothermal Conditions. *J. Am. Chem. Soc.* **2004,** *126*, 7790–7791.
20. Kakiuchi, K.; Hosono, E.; Imai, H.; Kimura, T.; Fujihara, S. {111}-Faceting of Low-Temperature Processed Rutile TiO_2 Rods. *J. Cryst. Growth* **2006,** *293*, 541–545.
21. Li, Y.; Guo, M.; Zhang, M.; Wang, X. Hydrothermal Synthesis and Characterization of TiO_2 Nanorod Arrays on Glass Substrates. *Mater. Res. Bull.* **2009,** *44*, 1232–1237.
22. Feng, X.; Shankar, K.; Paulose, M.; Grimes, Craig A. Tantalum-Doped Titanium Dioxide Nanowire Arrays for Dye-Sensitized Solar Cells with High Open-Circuit Voltage. *Angew. Chem., Int. Ed.* **2009,** *48*, 8095–8098.
23. Feng, X.; Shankar, K.; Varghese, O. K.; Paulose, M.; Latempa, T. J.; Grimes, C. A. Vertically Aligned Single Crystal TiO_2 Nanowire Arrays Grown Directly on Transparent Conducting Oxide Coated Glass: Synthesis Details and Applications. *Nano Lett.* **2008,** *8*, 3781–3786.
24. Liu, B.; Aydil, E. S. Growth of Oriented Single-Crystalline Rutile TiO_2 Nanorods on Transparent Conducting Substrates for Dye-Sensitized Solar Cells. *J. Am. Chem. Soc.* **2009,** *131*, 3985–3990.
25. Tian, Z. R.; Voigt, J. A.; Liu, J.; McKenzie, B.; Xu, H. Large Oriented Arrays and Continuous Films of TiO_2-Based Nanotubes. *J. Am. Chem. Soc.* **2003,** *125*, 12384–12385.
26. Enache-Pommer, E.; Boercker, J. E.; Aydil, E. S. Electron Transport and Recombination in Polycrystalline TiO_2 Nanowire Dye-Sensitized Solar Cells. *Appl. Phy. Lett.* **2007,** *91*, 123116–3.
27. Mor, G. K.; Varghese, O. K.; Paulose, M.; Shankar, K.; Grimes, C. A. A Review on Highly Ordered, Vertically Oriented TiO_2 Nanotube Arrays: Fabrication, Material Properties, and Solar Energy Applications. *Sol. Energy Mater. Sol. Cells* **2006,** *90*, 2011–2075.
28. Chi, B.; Jin, T. Synthesis of Titania Nanostructure Films *via* $TiCl_4$ Evaporation-Deposition Route. *Cryst. Growth Des.* **2007,** *7*, 815–819.
29. Wu, J.-M.; Shih, H. C.; Wu, W.-T.; Tseng, Y.-K.; Chen, I. C. Thermal Evaporation Growth and the Luminescence Property of TiO_2 Nanowires. *J. Cryst. Growth* **2005,** *281*, 384–390.
30. Wu, C.-W.; Ohsuna, T.; Kuwabara, M.; Kuroda, K. Formation of Highly Ordered Mesoporous Titania Films Consisting of Crystalline Nanopillars with Inverse Mesospace by Structural Transformation. *J. Am. Chem. Soc.* **2006,** *128*, 4544–4545.
31. Freer, E. M.; Krupp, L. E.; Hinsberg, W. D.; Rice, P. M.; Hedrick, J. L.; Cha, J. N.; Miller, R. D.; Kim, H.-C. Oriented Mesoporous Organosilicate Thin Films. *Nano Lett.* **2005,** *5*, 2014–2018.
32. Park, O.-H.; Cheng, J. Y.; Hart, M.; Topuria, T.; Rice, P. M.; Krupp, L. E.; Miller, R. D.; Ito, H.; Kim, H.-C. High Aspect-Ratio Cylindrical Nanopore Arrays and Their Use for Templating Titania Nanoposts. *Adv. Mater.* **2008,** *20*, 738–742.
33. Koganti, V. R.; Dunphy, D.; Gowrishankar, V.; McGehee, M. D.; Li, X.; Wang, J.; Rankin, S. E. Generalized Coating Route to Silica and Titania Films with Orthogonally Tilted Cylindrical Nanopore Arrays. *Nano Lett.* **2006,** *6*, 2567–2570.
34. Marzolin, C.; Smith, S. P.; Prentiss, M.; Whitesides, G. M. Fabrication of Glass Microstructures by Micro-Molding of Sol−Gel Precursors. *Adv. Mater.* **1998,** *10*, 571–574.
35. Hampton, M. J.; Williams, S. S.; Zhou, Z.; Nunes, J.; Ko, D.-H.; Templeton, J. L.; Samulski, E. T.; DeSimone, J. M. The Patterning of Sub-500 nm Inorganic Oxide Structures. *Adv. Mater.* **2008,** *20*, 2667–2673.
36. Schaper, C. D.; Miahnahri, A. Polyvinyl Alcohol Templates for Low Cost, High Resolution, Complex Printing. *J. Vac. Sci.Technol. B* **2004,** *22*, 3323–3326.
37. Schaper, C. D. Planarizing Surface Topography by Polymer Adhesion to Water-Soluble Templates with Replicated Null Pattern. *Langmuir* **2003,** *20*, 227–231.
38. Schaper, C. D. Patterned Transfer of Metallic Thin Film Nanostructures by Water-Soluble Polymer Templates. *Nano Lett.* **2003,** *3*, 1305–1309.

39. Crepaldi, E. L.; Soler-Illia, G. J. d. A. A.; Grosso, D.; Cagnol, F.; Ribot, F.; Sanchez, C. Controlled Formation of Highly Organized Mesoporous Titania Thin Films: From Mesostructured Hybrids to Mesoporous Nanoanatase TiO_2. *J. Am. Chem. Soc.* **2003,** *125*, 9770–9786.
40. Frot, T. C., S.; Laurent, G.; Sassoye, C.; Popall, M.; Rozes, L.; Sanchez, C. $Ti_8O_8(OOCR)_{16}$ a New Family of Titanium-oxo-clusters Potential NBUs for Reticular Chemistry. *Eur. J. Inorg. Chem.* **2010,** *36*, 5650–5659.
41. Joo, J.; Kwon, S. G.; Yu, T.; Cho, M.; Lee, J.; Yoon, J.; Hyeon, T. Large-Scale Synthesis of TiO_2 Nanorods *via* Nonhydrolytic Sol-Gel Ester Elimination Reaction and Their Application to Photocatalytic Inactivation of *E. coli*. *J. Phys. Chem. B* **2005,** *109*, 15297–15302.
42. Kim, Y. J. K.; Seok, Young; Chai, Seung Yong; Cha, Dong Hyun; Choi, Young Sik; Lee, Wan In Syntheses of Monodispersed SnO_2 and CeO_2 Nanoparticles through the Self-capping Role of 2-ethylhexanoate Ligands. *New J. Chem.* **2007,** *31*, 260–264.
43. Peng, C.; Pang, S. W. In *Hybrid mold reversal imprint for three-dimensional and selective patterning*, AVS: 2006; pp 2968-2972.
44. Yu, W. W.; Qu, L.; Guo, W.; Peng, X. Experimental Determination of the Extinction Coefficient of CdTe, CdSe, and CdS Nanocrystals. *Chem. Mater.* **2003,** *15*, 2854–2860.
45. Park, O.-H.; Cheng, J. Y.; Kim, H. S.; Rice, P. M.; Topuria, T.; Miller, R. D.; Kim, H.-C. Formation and Photopatterning of Nanoporous Titania Thin Films. *Appl. Phys. Lett.* **2007,** *90*, 233102–3.